www.advelectronicmat.de

Sustainable Soft Electronics Combining Recyclable Metal Nanowire Circuits and Biodegradable Gel Film Substrates

Yuxuan Liu, Mesbah Ahmad, Richard A. Venditti, Orlin D. Velev,* and Yong Zhu*

Direct disposal of used soft electronics into the environment can cause severe pollution to the ecosystem due to the inability of most inorganic materials and synthetic polymers to biodegrade. Additionally, the loss of the noble metals that are commonly used in soft electronics leads to a waste of scarce resources. Thus, there is an urgent need to develop "green" and sustainable soft electronics based on eco-friendly manufacturing that may be recycled or biodegraded after the devices' end of life. Here an approach to fabricating sustainable soft electronics is demonstrated where the expensive functional materials can be recycled and the soft substrate can be biodegradable. A stretchable agarose/glycerol gel film is used as the substrate, and silver nanowires (AgNWs) are printed on the film to fabricate the soft electronic circuits. The mechanical and chemical properties of the agarose/glycerol gel films are characterized, and the functionality of the printed AgNW electrodes for electrophysiological sensors is demonstrated. The demonstration of the biodegradability of the agarose/glycerol and the recyclability of AgNWs points toward ways to develop sustainable and eco-friendly soft electronics.

1. Introduction

Electronic waste (e-waste) poses a pressing threat to the health and environment, in large part because of the contamination of aquatic reservoirs with microplastics and inorganic particles released from e-waste.^[1–5] Currently, the process of degrading

Y. Liu, Y. Zhu

Department of Mechanical and Aerospace Engineering

North Carolina State University Raleigh, NC 27695, USA

E-mail: yzhu7@ncsu.edu

M. Ahmad, O. D. Velev

Department of Chemical and Biomolecular Engineering

North Carolina State University Raleigh, NC 27695, USA

Raleigh, NC 27695, USA E-mail: odvelev@ncsu.edu

R. A. Venditti

Department of Forest Biomaterials North Carolina State University Raleigh, NC 27695, USA



The ORCID identification number(s) for the author(s) of this article can be found under https://doi.org/10.1002/aelm.202300792

© 2024 The Authors. Advanced Electronic Materials published by Wiley-VCH GmbH. This is an open access article under the terms of the Creative Commons Attribution License, which permits use, distribution and reproduction in any medium, provided the original work is properly cited

DOI: 10.1002/aelm.202300792

the e-waste from electronic devices releases microplastics, dispersed particulate polymer debris that has accumulated in large amounts in the oceans and freshwater systems, creating vast environmental problems.[6-14] Similarly, the inorganic particles used in the composite materials of the circuit boards can be released in the form of finely dispersed nano and microparticles, which pose an environmental concern due to their ability to be ingested and accumulate in animals and humans.[15] The problem is further exacerbated by the presence of toxic and hazardous components in some electronic devices.[16,17] On the other hand, the present ways of manufacturing electronic devices accelerate the exhaustion of already scarce natural elements including noble metals.^[6,18,19] There is an urgent need for eco-friendly manufacturing of sustainable electronics,

based on the recycling of precious functional materials and biodegradation or recycling of other materials.

The field of soft electronics has emerged in recent years in parallel to conventional Si-based "rigid" electronics. Soft electronic systems that are flexible, stretchable, and imperceivable to users have enabled a wide range of applications from wearable health monitoring to next-generation robots.^[20–29] As an example, soft wearable sensors for monitoring vital physiological signals, including pulse rate, respiration rate, skin temperature, and blood pressure, make possible personalized medicine wherein an individual's health status can be continuously monitored and evaluated.^[30,31] Soft wearable sensors can interface conformally with the human skin and flex in response to human movement. It is timely to develop sustainable materials for soft electronics for such emerging applications.

Transient electronics, which are physically disintegrated and/or dissolved at the end of their life, can form the basis of many applications ranging from wearable and implantable medical devices to field deployable environmental sensors. [6,10,14,32,33] While of large interest, not all materials used presently in such devices are biodegradable, which can still lead to environmental concerns. In addition, the classes of electronic components used to date do not enable true recycling of the functional materials. In the recent few years, a more elaborate concept of recyclable soft electronics has emerged. For example, Zou et al. reported recyclable conductive nanocomposites with nanoparticles doped in a polymer matrix. [11] Williams et al. reported printable and recyclable carbon electronics. [12] Shi et al. reported





www.advelectronicmat.de

multifunctional wearable electronic system that can recycle both the polyimine substrate and the liquid metal which is an alloy of Gallium and Indium.^[34] Liu et al. reported the recycling of metal nanowire networks for soft electronic devices.^[35] Jaiswal et al. reported cellulose nanocomposite as the substrate and were able to recover electronic components from the printed samples.^[36] Qi et al. developed flexible perovskite solar cells using PGS substrates. They were able to biodegrade these substrates while the silver nanowires (AgNWs) could be recycled.^[37] However, sustainable soft electronics that simultaneously recycle functional materials and utilize biodegradable substrates have hardly been reported.

Over the past few years, there has been a significant interest surrounding biomaterials, owing to their biodegradability, renewability, biocompatibility, and promising applications in the field of electronics.[38] Herein, we report a strategy to fabricate and test prototypes of sustainable soft electronics by using a renewable and biodegradable substrate material (agarose/glycerol gel film) onto which we print recyclable functional materials (silver nanowires). Agarose is a naturally derived biodegradable polymer.[39] Glycerol is a byproduct of biofuel synthesis with high thermal stability, which is widely used as an effective plasticizer for biopolymers.^[40] The biopolymer gel film decorated with the printed AgNW electric circuits is intrinsically stretchable. The biodegradability of the agarose and recyclability of AgNWs lead to eco-friendly manufacturing of sustainable soft electronics. In order to match the mechanical characteristics of human skin, the stiffness of the agarose/glycerol gel film is tailored by adjusting the glycerol plasticizer/agarose ratio. The mechanical and chemical properties of the agarose/glycerol films are characterized to understand the role of the material's structure and composition. Other key factors related to the requirements for soft wearable applications such as optical transmittance, water vapor transmission rate, swelling behavior, and thermal properties are evaluated. Then, the AgNWs are printed on the agarose substrate to fabricate soft electrodes. The electromechanical properties of the printed electrodes, including stretchability, durability, and stability in different media, are investigated. The electrodes are used to record electromyography (EMG) signals of the brachioradialis muscle, which are used to control a motor toy as a demonstration of the human-machine interface. The sustainability of the printed soft electronics is achieved by biodegrading the agarose/glycerol substrate and recycling the AgNWs.

2. Results and Discussion

2.1. Fabrication of the Biodegradable Gel Film Substrate

A schematic overview of our approach to sustainable soft electronics is illustrated in **Figure 1a**. First, we form soft gel films from plasticized agarose, which are then used as substrates for the printed recyclable circuits. The agarose gel films are fabricated by a facile and eco-friendly process. Agarose and glycerol at a certain ratio are mixed with hot water to form a clear viscous solution. The solution cools down to room temperature in a mold during which it gels. Further, the excess water evaporates slowly to form a thin gel film, as shown in Figure 1b. More details on the fabrication process of the gel films are provided in the Experimental Section.

Agarose solutions in water exhibit sol-gel transition behavior. When agarose is exposed to water heated above 85 °C, it dissolves in a molecular state of random chains or coils. When the temperature reaches ≈35 °C upon cooling, gelation occurs, and agarose chains form intramolecular and intermolecular hydrogen bonds resulting in a 3D network of helical fiber bundles. [41-43] Glycerol molecules have three hydroxyl groups that form hydrogen bonds with the agarose chains and helices. The molecular structure of the formed gel film is schematically shown in Figure 1c. The agarose/glycerol gel film fabricated by this process is soft and stretchable. It can be stretched to over 60% strain, as shown in Figure 1d. The film is optically transparent, as illustrated against a clearly visible background (Figure 1e). Qualitatively, the film shows outstanding conformability and adhesivity to human skin, thus representing a promising candidate substrate for wearable devices (Figure 1f). The physical origins of the strong adhesivity of the glycerol-plasticized agarose to skin could be of importance in the development of wearable devices, but are outside the scope of this report.

2.2. Structure and Properties of the Gel Film Substrate

The type and concentration of the plasticizer in the gel matrix play a critical role in controlling its mechanical and surface properties. As illustrated in **Figure 2a**,b, the agarose chains are stabilized by intramolecular and intermolecular hydrogen bonds between the macromolecules. When glycerol is introduced as a plasticizer, the glycerol molecules form intermolecular hydrogen bonds with the agarose chains adding free volume and thus increasing the molecular mobility of the polymers. The optical transmittance of the agarose gel films with different glycerol ratios is shown in Figure 2c. The films have outstanding optical transparency; for example, the transmittance values at the wavelength of 550 nm are 92.3% and 90.5% for agarose/glycerol weight ratios of 1:3 and 1:5, respectively.

To probe the molecular interaction mechanisms in the agarose films with different glycerol ratios, the Fourier-transform infrared spectroscopy (FTIR) spectra of the glycerol solvent, the pure agarose powder, and the gel film with agarose/glycerol weight ratio of 1:1, 1: 5, and 1:7 were collected. As shown in Figure 2d, the signals in the range of 1000–4000 cm⁻¹ indicate the typical bonds of alcohol and ether; the peaks in the 650-1000 cm⁻¹ range are typical of anomeric carbon and pyranose rings in agarose.[44] The asymmetrical and symmetrical C-H stretching vibrations in glycerol and agarose appear at 2938 and 2886 cm⁻¹, respectively.^[45] It can be seen that the spectra from pure glycerol and agarose are too close to be precisely differentiated. However, with increasing glycerol content in the matrix, two featured peaks (≈3300 and ≈1050 cm⁻¹) show prominent changes. In the spectra of pure agarose and agarose with glycerol plasticizer, the peaks at $\approx 1040 \text{ cm}^{-1}$ can be assigned to the C-O stretching vibrations in agarose. [46] The peak located at 1025 cm⁻¹ is for pure glycerol. The intensity increases significantly when the glycerol/agarose ratio increases, and the location of the peak shifts from 1039.9 cm⁻¹ (pure agarose) to 1044.8 cm^{-1} (agarose/glycerol: 1:5). These features indicate the formation of a larger number of intermolecular hydrogen bonds when the glycerol mass fraction increases.

www.advelectronicmat.de

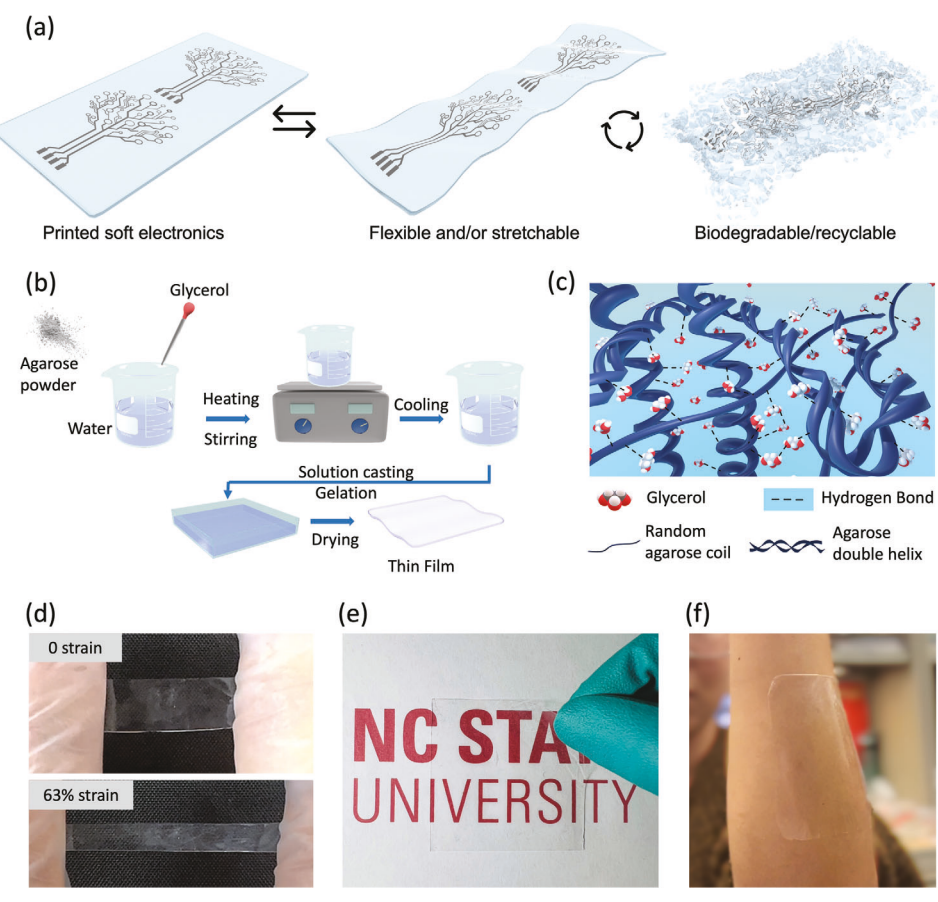


Figure 1. a) Schematic diagram of the sustainable soft electronic circuits investigated here. b) Fabrication process of agarose/glycerol gel film. c) Schematic diagram of the polymer matrix of the fabricated gel. d) Initial and stretched states of the agarose/glycerol gel film. e) Transparency demonstration of the film. f) A 15 cm \times 15 cm square-shaped gel film conformably attached to human skin.

Further information elucidating the molecular structure of the gel film can be found in the shift of the peaks in the range of 3000–3600 cm⁻¹ representing the C—OH hydroxy groups. Pure glycerol has a single peak at 3350 cm⁻¹. The agarose has broad dimeric bands at 3527.7 and 3225.9 cm⁻¹, which, when plasticized with glycerol at the ratio of 1:1, shift to 3515.2 and 3167.6 cm⁻¹, respectively, indicating the formation of intramolecular (3515.2 cm⁻¹) and intermolecular (3167.6 cm⁻¹) hydrogen bonds.^[47,48] With a further increase in the glycerol fraction (agarose/glycerol weight ratio to 1:5 and 1:7), these two peaks become narrower at 3378.2 and 3390.8 cm⁻¹, respectively. The blue shift observed with an increase in the glycerol content, indicates formation of numerous intramolecular and intermolecular hydrogen bonds.^[45]

Tensile tests were carried out to evaluate the mechanical properties of the agarose/glycerol gel films with different ratios, as shown in Figure 2e. It can be seen that the incorporation of glycerol reduces the tensile stress, imparting softness to the film. By increasing the agarose/glycerol ratio from 1:0.5 to 1:5, the tensile stress reduced from 34.2 MPa to 978 kPa, which is within the same order of magnitude as that of human skin. At the same time, the stretchability of the gel film increased from 24.8% to 68.1%. The mechanical behavior transformed from the typical plastic type to the gel type with the increase of the plasticizer.

When the agarose/glycerol ratio increased to 1:6 and 1:7, the mechanical performance deteriorated, showing lower stretchability and stress. When this ratio increased further, the samples became too soft to be clamped for the tensile test.

The enhancement of the mechanical stretchability of the agarose/glycerol gel films can be attributed to the extensive hydrogen bonds formed between the hydroxyl groups (—OH) of glycerol and agarose chains. These hydrogen bonds could efficiently dissipate energy and prevent crack propagation during stretching and as a result, enhance stretchability. [49] Hydrogen bonds between polymer-polymer are interrupted by hydrogen bonds between glycerol and polymer, thus providing more mobility of the polymer chains, since large polymer sections do not need to move in a coordinated fashion. However, high glycerol content in the gel film could lead to gel brittleness due to the loss of agarose intermolecular connections. Therefore, we found that the agarose/glycerol ratio optimizing high stretchability is $\approx 1:5$.

Young's modulus is a very useful characteristics for soft electronics applications. Figure 3a shows the change in Young's moduli of the agarose gel films with different glycerol content. Young's modulus significantly reduces with increase in the glycerol concentration in the gel matrix. In this respect, it is useful to compare the mechanical properties of our films to the common silicone devices and to human skin in terms of Young's

ADVANCED ELECTRONIC MATERIALS

www.advelectronicmat.de

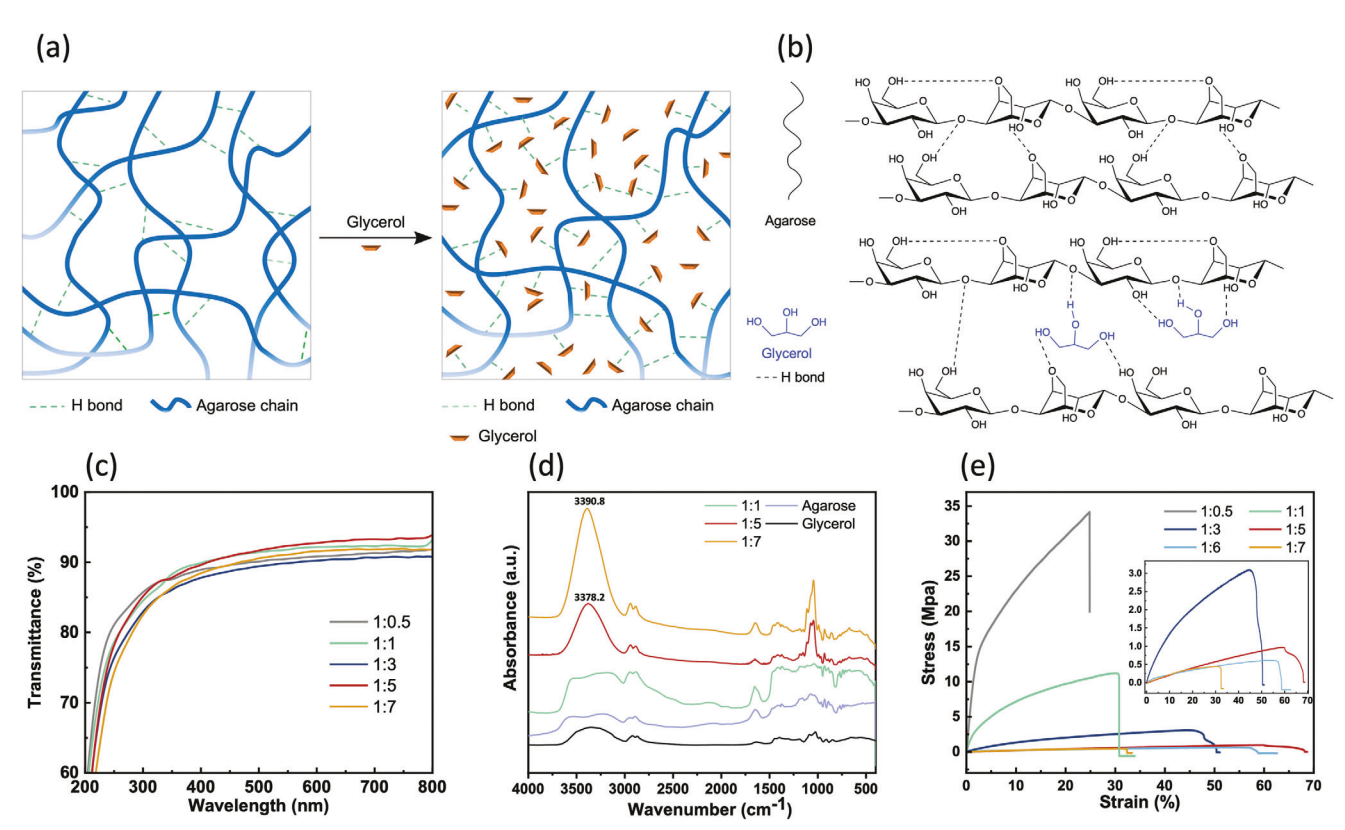


Figure 2. a) Schematic illustration of the matrix of the agarose gel film with and without glycerol. b) Hypothesized chemical structure of the film with intramolecular and intermolecular hydrogen bonds. c) UV-vis spectra of the gel films with different agarose/glycerol ratios ranging from 1:0.5 to 1:7 indicating high transmittance in the visible light spectrum. d) FTIR spectra of the gel films with different agarose/glycerol ratios (1:1, 1:5, and 1:7), pure agarose powder, and pure glycerol indicating an increased number of H-bonds at larger glycerol fractions. e) Tensile test of the gel films with different agarose/glycerol ratios showing increased softness and stretchability at larger glycerol fractions. The inset shows a magnified view of the low-stress range.

modulus (Figure S1, Supporting Information). The agarose film 1:5 exhibits a Young's modulus of 1.86 MPa, while Young's modulus of pure polydimethylsiloxane (PDMS) falls within the range of 1.32 to 2.97 MPa.^[50,51] The submandibular neck and forearm skin tissues were reported to have Young's modulus of 1.28 and 1.03 MPa, respectively, in the same order of magnitude as the agarose substrate.^[52] In comparison to agarose 1:5 film, Young's modulus of the agarose 1:7 film further reduces to 1.82 MPa. However, the tradeoff is that the stretchability, another important mechanical property, of the film deteriorates.

Strain recovery is another important parameter for soft electronics. The residual strain of an agarose film was measured after stretching the film to the designated strain, releasing the film, and resting for 10 min. As shown in Figure 3b, when the glycerol ratio was in the range of 1:0.5 to 1:5, the residual strain decreased with the increasing glycerol content. At a higher ratio of up to 1:7, the residual strain increased further, indicating the deterioration of the reversibility. The results further confirmed that the 1:5 agarose/glycerol ratio offers the most favorable mechanical behavior. Hence, this ratio was used in the rest of this study. The residual strain can have an impact on the performance of the electronic patches. However, the agarose/glycerol 1:5 film shows negligible residual strain at applied strains up to 10%. The AgNW circuits can maintain stable function under such a low strain.

Indeed, for most skin wearable applications (except joints), the strain that the skin undergoes is small. For applications requiring larger strain ranges, stretchable structures such as wrinkles and kirigami can be employed. [53,54] The strain recovery phenomenon is a result of a complex interaction between entropy and elastoplastic deformation, which can be optimized in the future.

Water vapor permeability is another key parameter used to evaluate the applicability of agarose/glycerol gel films in wearable electronic devices on human skin, which require "breathability". The water vapor transmission rate (WVTR) was measured with gel films with different agarose/glycerol ratios. A PDMS film with the same thickness was measured as a baseline standard. Figure 3c shows the water vapor transmission rate results conducted for 40 h. The water vapor transmission values for the films with change in time are shown in Figure S2 (supporting information). It can be seen that the transmission rate (shown in the left Y axis in Figure 3c) increases with the increasing concentration of glycerol in the matrix. Even the lowest WVTR corresponding to the 1:0.5 ratio shows a higher value than that of PDMS, indicating that the agarose/glycerol gel films possess superior water vapor permeability. WVTR of the agarose/glycerol gel film with the ratio of 1:5, which has the best mechanical properties, was 31.92 mg cm⁻² h⁻¹. This is comparable to our previously reported porous elastomer material.[55]



www.advelectronicmat.de

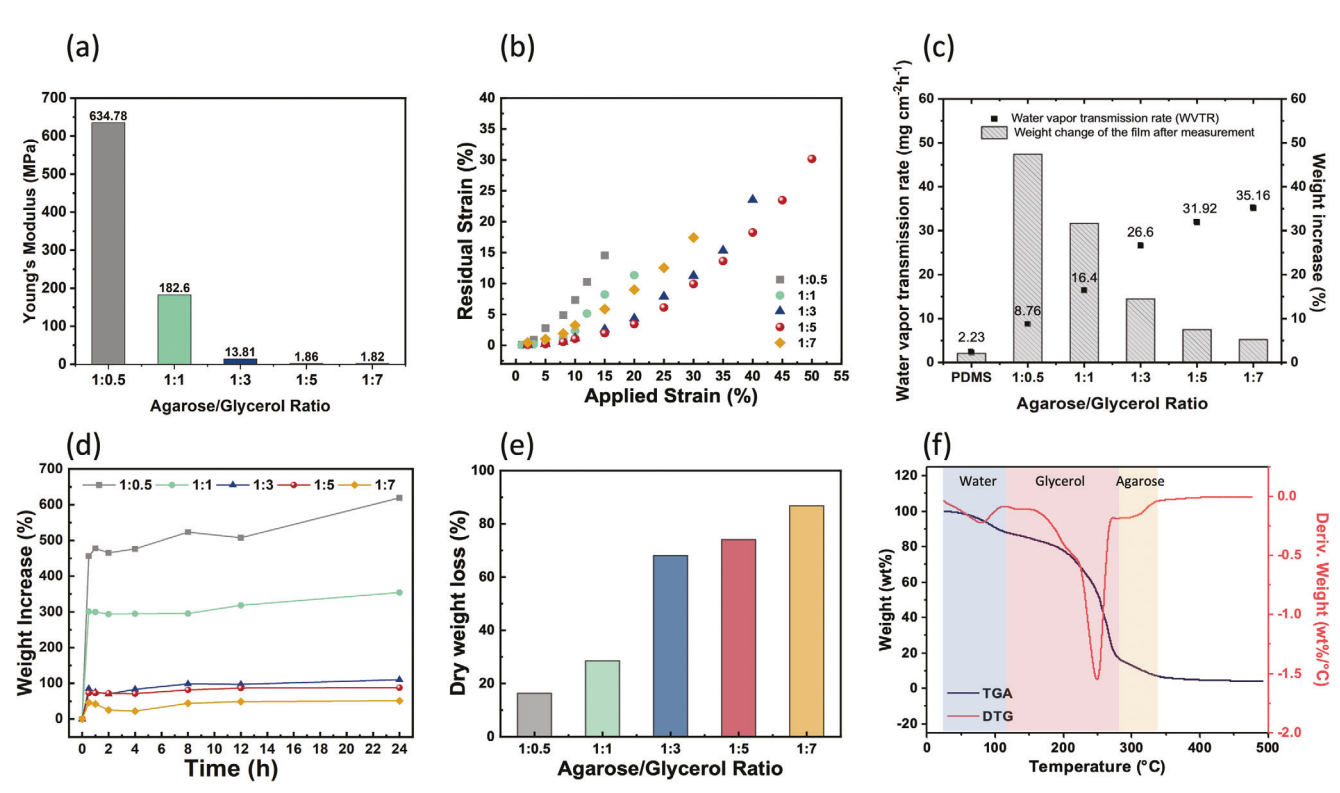


Figure 3. a) Young's modulus of the gel films with different agarose/glycerol ratios. b) Residual strain test results of the films with different agarose/glycerol ratios. c) Water vapor transmission rate results and the weight change of the gel films with different agarose/glycerol ratios indicating a higher water vapor transmission rate with an increase in glycerol content. d) Weight increase of the gel films with different agarose/glycerol ratios after immersing in water for 24 h. e) Dry weight loss of the gels with different agarose/glycerol ratios after leaching experiments in water showing higher weight loss for larger glycerol fractions. f) TGA and DTG results of the gel films with agarose/glycerol ratio of 1:5.

WVTR relies on both the migration rate and the evaporation rate of water. In the transmission process, the water vapor is initially absorbed on one side of the film and then migrates to the other surface of the film to evaporate. Considering the high solubility of water in glycerol, we expect that the migration rate of water increases with the glycerol content in the polymer matrix. The high affinity between water and glycerol present in the matrix facilitates the migration of water molecules. The evaporation rate depends on the concentration of water molecules on the surface of the film and the ambient environment. When the glycerol content is relatively low, migration becomes the rate-limiting step in the water vapor transmission process, due to the lower migration rate of the water molecules in the gel film. At a higher glycerol concentration, surface evaporation can become the rate-limiting step, which explains why the WVTR of the film with a ratio of 1:7 did not increase significantly compared to that of the film with a ratio of 1:5.

The weight change of the gel films after 40 h of water vapor exposure was measured and plotted on the right Y axis in Figure 3c. As the glycerol content increases, the relative film weight change increases. The smaller weight change (or less absorbed water) is likely a result of the increased migration rate of water. This further corroborates that the migration rate increases with the glycerol content in the gel. It is worth noting that the WVTR testing configuration represents a good model for the practical applications of wearable epidermal electronics, where one side of the substrate faces the skin with sweat absorp-

tion, and the other side faces the air enabling evaporation of the water.

To further investigate the water absorption behavior of the agarose/glycerol gel films, samples were immersed in DI water for 24 h. The films were then taken out of the water, blotted, and their corresponding change in weight was measured and shown in Figure 3d. The gel film with a lower glycerol content shows higher relative water absorption, as indicated by the larger weight increase. The sample with a 1:0.5 ratio shows a weight increase of 619%, while the sample with a 1:7 ratio only shows a 51% increase in weight after 24 h of water intake. This result is consistent with the WVTR measurement where the weight increase was higher for the gel films with lower glycerol content. When the matrix contains a high fraction of glycerol, the migration flux of these glycerol molecules from the film surface to the surrounding water increases (i.e., more glycerol leaches into the water). The water absorption also introduces volume change to the agarose/glycerol gel films, as shown in Figure S3 (supporting information). The volume change decreases with the increase of the glycerol ratio. Somewhat counterintuitively, this indicates that gel films with higher glycerol ratios are more stable in terms of maintaining their initial dimensions when exposed to water, relevant in situations when epidermal electronics come into contact with sweat on the skin.

The dry weight loss of the agarose/glycerol gel films after soaking in water and drying in the oven at 60 $^{\circ}$ C for 24 h is shown in Figure 3e. It can be seen that the weight loss is larger for





www.advelectronicmat.de

the film with a higher glycerol content. For the film with an agarose/glycerol ratio of 1:0.5, there is a 16.3% weight loss likely due to the leaching of glycerol into the surrounding water. With the agarose/glycerol ratio of 1:7, the dry weight loss of the gel film increases to 86.8%.

TGA and derivative thermogravimetry (DTG) were further used to characterize the ratio of water, glycerol, and agarose in the gel film with the agarose/glycerol ratio of 1:5. As shown in Figure 3f, the initial degradation occurs around 70–140 °C with $\approx \! 14.5\%$ weight loss, which can be attributed to the loss of water due to evaporation. The second decomposition stage is observed $\approx \! 140-290$ °C with $\approx \! 73\%$ weight loss, which likely corresponds to the evaporation and decomposition of glycerol. The final degradation stage of the gel occurs around 290–350 °C, due to the denaturization and decomposition of the agarose matrix. After complete degradation, the ash content of the gel film is recorded as 4%.

2.3. Printing of AgNW Circuits on Agarose/Glycerol Gel Film Substrate

The conductive AgNW patterns were printed on the agarose/glycerol gel film substrate using screen printing following our previous process, as schematically shown in Figure 4a. [56] The ink composition consisted of AgNWs dispersed in a medium formulated by 4% poly(ethylene oxide) (PEO) dissolved in a mixed solvent with a 50:50 ratio of ethanol and deionized water. The resulting conductive patterns were 100 μ m-300 μ m wide and \approx 4 μ m thick. The resistance of a printed line with 150 µm width, 2 cm length, and 4.5 µm thickness was 8.6 ohm, and the conductivity was measured to be 3.45×10^6 S m⁻¹. The gel film with printed electrodes showed excellent mechanical stretchability and could be mounted on the skin for testing of epidermal electronics applications (Figure 4b). After peeling off the mounted electrode from the skin, there is no visible damage of both the electrode/gel film substrate and the skin. The resistance of the electrode after repeated peeling off up to 100 times is shown in Figure S4 (Supporting Information).

To evaluate the printability of the AgNW-based inks on the gel film, the static contact angles of water, AgNWs/ethanol solution, and AgNWs/PEO ink on the film were measured and compared to those on the PDMS substrate. As shown in Figure 4c, PDMS has higher contact angles with all the probing liquids due to its low surface energy. The gel film shows overall lower contact angles, especially with water, attributed to the hydrophilicity of agarose and glycerol. The contact angle between the gel film (ratio of 1:5) and the AgNWs/PEO ink shows a moderate value (*90°) that is suitable for screen printing – low enough for ink settling but high enough to prevent ink spreading.

The electromechanical properties of the printed electrodes were investigated. The resistance change of a printed line pattern under a tensile loading-unloading cycle is shown in Figure 4d. For instance, when 20% strain is applied to the printed pattern, the resistance increases by 55%. After releasing the strain, it decreases to ≈11% indicating good stretchability of the printed electrode. The 11% residual resistance increase was after the first unloading from the 20% strain. The strain shown in Figure 4d was increased progressively. For the strains from 2.5% to 15%,

the second loading and the first unloading followed the same resistance-strain path, suggesting reversible resistance versus strain. If the sample is loaded again to 20%, it would follow the same resistance-strain path. This behavior has been reported in the literature.^[57] The cyclic tensile test up to the strains of 2%, 5%, and 10% were carried out and the resistance change in 100 cycles was recorded, as shown in Figure 4e. It can be seen that the electromechanical reversibility of the printed electrode on the gel film is excellent when the applied strain is within 5% but deteriorates when the applied strain is 10%. Adhesion between the printed AgNW pattern and the gel substrate needs to be strong to maintain robust electromechanical properties. Figure 4f shows a scanning electron microscopy (SEM) image of the cross-section of the printed AgNWs on the agarose gel film. The interface between the AgNWs and the film appears to be strong and tight as a result of the good wettability between the ink and the substrate. This confirms that the PEO used in the ink serves as an effective binder to provide stronger adhesion. To further increase the reversibility range of the electromechanical properties, an encapsulation layer can be applied to protect the conductive pattern.^[20] In this work, we did not include such an encapsulation layer in order to enable the direct contact of the electrodes with the skin, as needed for the electrophysiological sensor applications that are demonstrated later.

Stretchable electrodes with strain-insensitive interfacial impedance are desirable for epidermal electronics. Figure 4g shows the electrode-skin impedance under different strains from 0 to 25%. The serpentine-shaped electrode shows a nearly constant impedance profile within 25% strain. For example, under 10% strain, there is a ≈80% and 140% impedance increase for an AgNW electrode on the agarose gel film substrate measured at 1 kHz and 1 Hz, respectively. Apart from the electromechanical stability under strain, the electrodes should be stable in commonly used media. The resistance changes of the printed electrodes were measured in the ambient environment (air), DI water, ethanol, and artificial sweat for 200 h, as shown in Figure 4h. The resistance changes are \approx 4% in all cases. The electrode soaked in ethanol shows a slight decrease in resistance, probably caused by shrinkage of the substrate due to loss of plasticizer that introduces compression of the electrode and improves the contact between AgNWs. The electromechanical stability and the chemical stability of the printed AgNW electrode on an agarose gel film substrate demonstrate its promise to be used in long-term wearable soft electronic applications. Furthermore, the stability of the device in ethanol makes it feasible to sterilize used devices for reuse without performance deterioration.

2.4. Application as Sustainable Electronic Patches

Electronic sensors or patches can demonstrate their broad utility in various applications—ranging from environmental monitoring with gas sensors to precise medical diagnostics using biosensors, showcasing the adaptability and impact of electronic sensing technologies. [58,59] To demonstrate potential applications of the printed AgNW electrodes on the agarose substrate in health monitoring, we used them to collect the electrocardiogram (ECG) signal of humans. **Figure 5**a shows one of the three electrodes



www.advelectronicmat.de

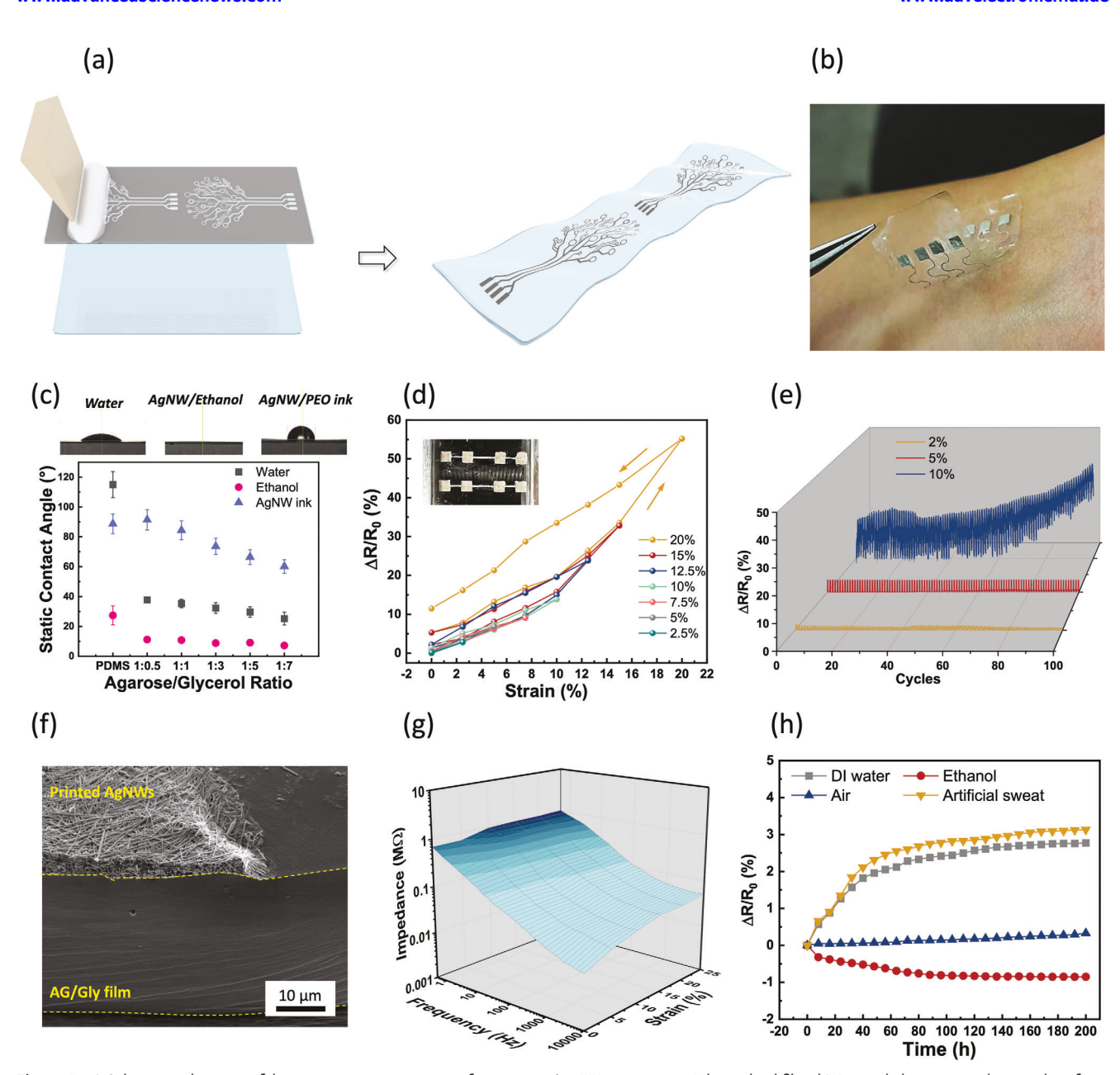


Figure 4. a) Schematic diagram of the screen-printing process for printing AgNWs on agarose/glycerol gel film. b) Printed electronics when peeling from the skin. c) Contact angle between the different ink probe liquids and the agarose/glycerol films with different ratios. PDMS was used as a comparison. d) Resistance changes of the printed AgNW straight lines on agarose/glycerol gel film with the ratio of 1:5 when loading and unloading different tensile strains. e) Cyclic tensile test of the printed electronics under 2%, 5%, and 10% strain. f) SEM image of the cross-section of the printed electronics with AgNW pattern on agarose/glycerol gel film. g) Impedance of the printed electrode when different tensile strain is applied. h) Resistance changes of the printed electrode immersed in different media including air, water, ethanol, and artificial sweat.

attached to the wrist with good conformability. These electrodes do not delaminate under stretching, compressing, and twisting of the local skin, as shown in Figure 5b–d. The electrodeskin impedances of AgNWs on agarose gel film, AgNWs embedded in PDMS, and commercial gel electrodes were measured for comparison (Figure 5e). The AgNW/agarose electrodes show an impedance similar to that of the commercial gel electrodes and slightly lower than that of the AgNW/PDMS electrodes, which can be attributed to the excellent conformability of the

AgNW/agarose gel film. The ECG signals measured by the AgNWs/agarose film electrodes and the commercial gel electrodes are compared in Figure 5f, showing no noticeable difference.

An electromyography (EMG) electrode array was constructed to detect the brachioradialis muscle's contraction during weightlifting. The three-electrode array attached to the muscle is shown in Figure 5g. Figure 5h compares the rectified EMG signal acquired from the AgNW/agarose gel film electrodes and the commercial gel electrodes when a subject lifted different

com/terms-and-conditions) on Wiley Online Library for rules of use; OA articles are governed by the applicable Creative Commons License

www.advelectronicmat.de

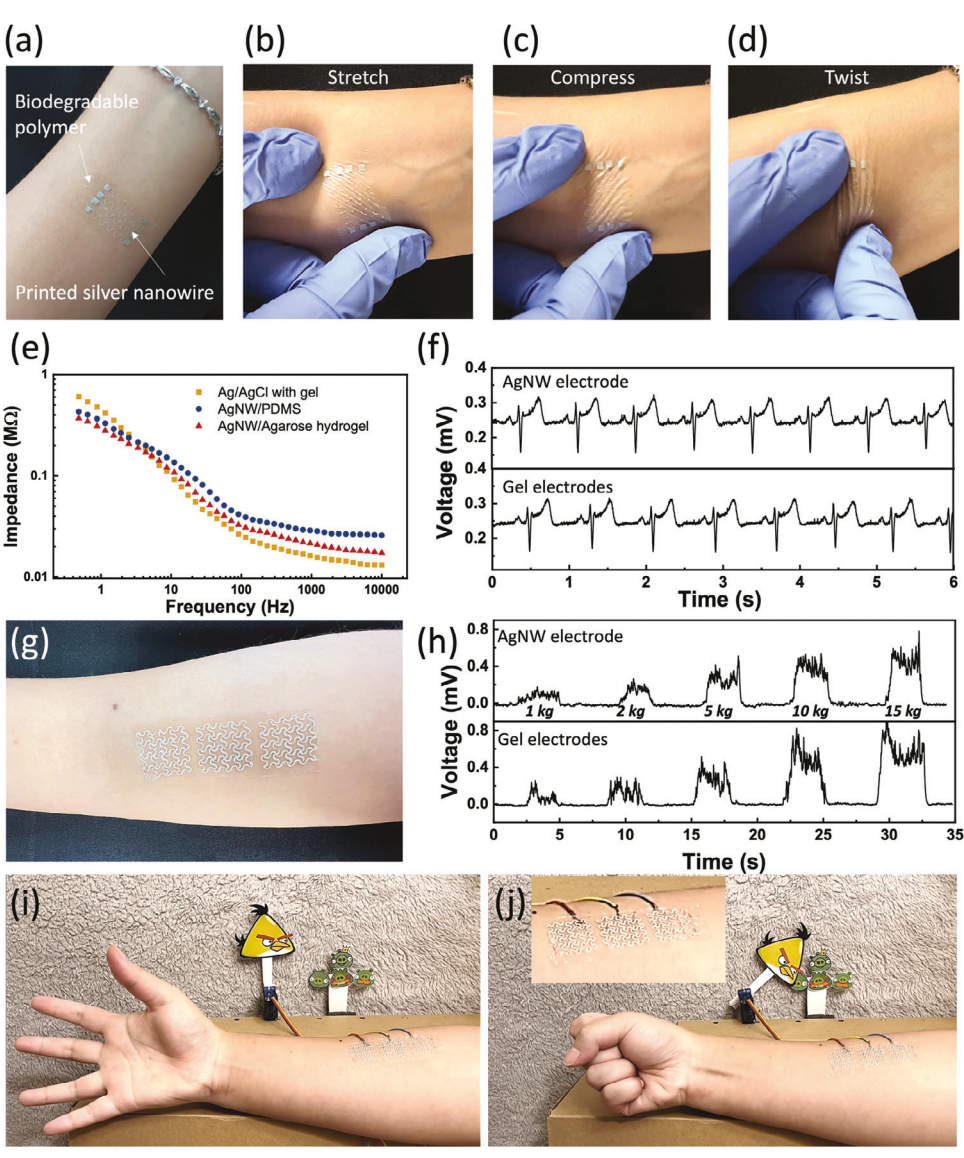


Figure 5. a) AgNW/agarose gel film electrode patch mounted on arm. b—d) AgNW/agarose electrodes on skin when being stretched, compressed, and twisted, respectively. e) Electrode-skin impedances of AgNW/Agarose gel film electrode, AgNW/PDMS electrode, and commercial gel electrode. f) ECG signals of AgNW/Agarose gel film electrodes (with agarose/glycerol ratio of 1:5) and commercial gel electrodes for comparison. g) EMG electrode array mounted on brachioradialis muscle. h) Rectified EMG signals of AgNW/Agarose gel film electrodes and commercial gel electrodes for comparison. i) Example of haptic control via the EMG electrode array. The motor toy stays at an angle of 90° when the muscle relaxes. j) The motor toy goes to an angle of 60° when the muscle contracts.

weights ranging from 1 to 15 kg. Larger weight results in a stronger contraction of the muscle and hence a larger signal magnitude. No obvious difference exists in the EMG profiles of the two types of electrodes. Furthermore, a muscle-controlled servo motor system was applied to demonstrate the application of the EMG electrodes for the human-machine interface. A threshold of 0.2 mV in magnitude of the EMG signal was preset. When the EMG signal was lower than the threshold, the servo motor stayed at 90° (with respect to the horizontal axis); when the signal was higher than the threshold, the servo motor rotated to 60°. On this basis, a control scenario was devised wherein the contraction of the brachioradialis muscle, triggered by gripping the palm, results in the "angry bird" rotating to strike the "pig",

as shown in Figure 5i,j. The printed AgNW/agarose gel film electrodes were used to collect the EMG signal, as shown in the inset in Figure 5j, which was transmitted to the processing board to control the rotation of the "angry bird".

2.5. Microbial Biodegradation and Recycling

At the end of life, the gel film substrate can undergo biodegradation, while the functional AgNWs can be recycled. The biodegradability of the gel film substrate was assessed by means of aerobic microbial degradation. For comparison, a sterile silver nanowire electrode was immersed in DI water as a control, while a second



www.advelectronicmat.de

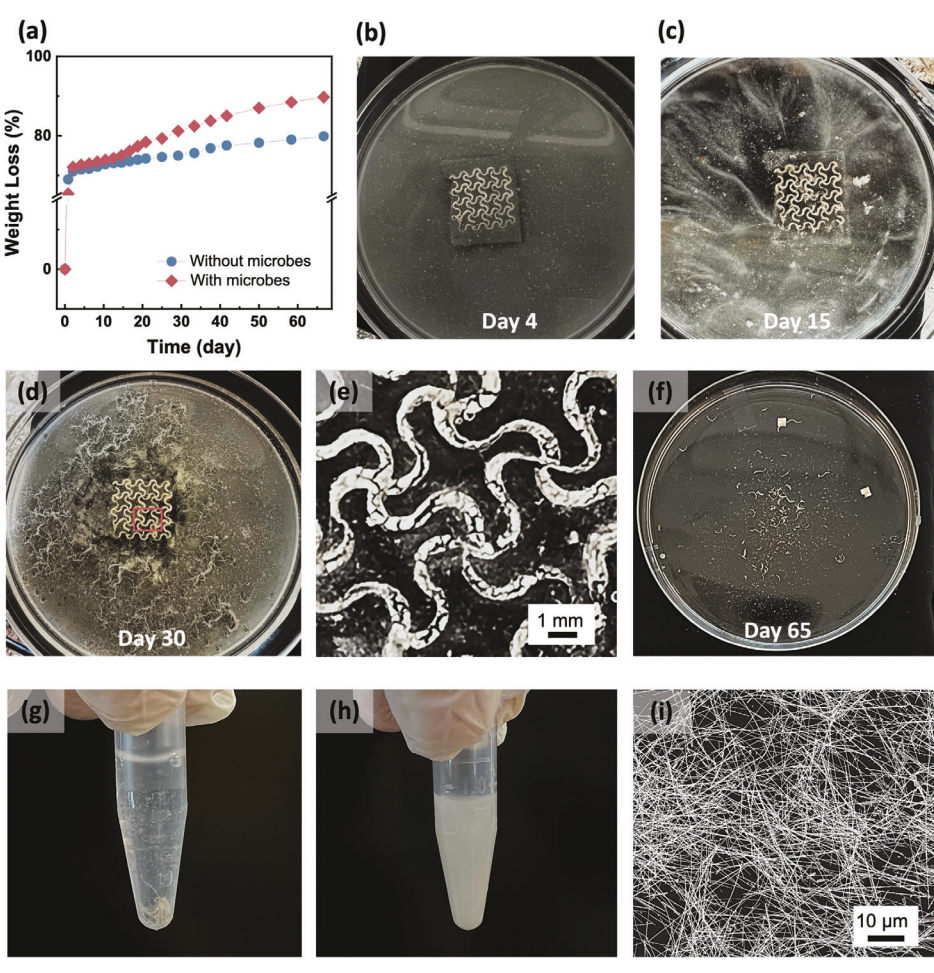


Figure 6. a) Weight loss of the two samples in the microbial environment and the DI water without microbes. b—e) A series of photographs taken on the 4th, 15th, and 30th days after starting the degradation process. e) Magnified view of the electronic patch on the 30th day. f) AgNW fragments precipitated at the bottom of the Petri dish after removing the microbial communities and the nondegraded substrate. g) Collected AgNWs in suspension. h) Ultrasonicated AgNW dispersion. i) SEM image of the recycled AgNWs from the ultrasonicated AgNW dispersion.

identical electrode was immersed in a microbial suspension formulated by a commercial compost activator. Details of the experiment can be found in the Experimental Section. Figure 6a shows the weight loss of the two electrodes (when picked out of the solutions and dried) versus the days of immersion in the solution. The initial large loss in weight is due to the rapid leaching of the glycerol, similar to the data in Figure 3e. For the control sample, the weight decreases slowly and remains almost constant after 40 days. The experimental group in the microbial solution shows a similar trend to the control group but with more rapid weight loss. This can be attributed to the biodegradation of the agarose, which not only decreases the weight of the agarose in the gel film but also releases the bonded glycerol from the matrix; both can contribute to weight loss.

A series of pictures taken during the process of microbial growth and biodegradation from the 4th day to the 30th day are shown in Figure 6b–e. It can be seen that the microbial communities grew well in the system. The weight loss accelerates after 15 days, which may be due to the ascendancy of metabolically efficient species of the microbial population. After 30 days, the substrate of the electrode started to disintegrate, and cracks formed

across the printed AgNW pattern. After 65 days, the floating microbial communities on the surface of the water and fragments of the nondegraded substrate were removed, leaving AgNW fragments precipitating at the bottom of the Petri dish, as shown in Figure 6f. The AgNW fragments were collected and centrifuged 3 times in ethanol to further remove the residues of the microbial community (Figure 6g). Then redispersion and recycling of the AgNWs were carried out using ultrasonication based on the technique reported previously,^[35] as shown in Figure 6h. SEM image of the recycled AgNWs, drop cast on a substrate (Figure 6i), indicates that the recycled NWs maintained the desired morphology to be printed again for new device fabrication.

3. Conclusion

This report presents a class of sustainable soft electronic circuits where expensive and nonrenewable functional materials can be recycled and the biopolymer substrates are biodegradable. The soft electronic devices consist of printed recyclable AgNW circuits onto biodegradable agarose-based gel film substrates. To adapt to the epidermal electronics applications, the agarose



www.advelectronicmat.de

gel film was modified by a glycerol plasticizer to achieve excellent mechanical stretchability, reversibility, and durability. The properties relevant to the making of these substrates, including molecular interactions, water vapor permeability, water absorption, plasticizer leaching, and thermal degradation were characterized, and the efficacy of the modified agarose/glycerol gel films as multifunctional substrates for epidermal soft electronics was confirmed. Conductive AgNW electrodes were screen printed on the biodegradable gel films, exhibiting high electromechanical stability and chemical stability in air, water, and model sweat and strain-insensitive low impedance at the electrode/skin interface. The printed electrodes demonstrated excellent performance as electrophysiological sensors for human health monitoring and human-machine-interface applications. Furthermore, we demonstrated that the agarose/glycerol substrate can be biodegraded and the printed AgNWs can be recycled at the end of the life. The approach reported in this work could in the future be extended to additional circuit functionalities by adding biodegradable organic semiconductor elements or other recyclable soft electronic components involving functional nanomaterials. While this study has provided numerous insights into developing sustainable soft electronics, it also reveals certain limitations, such as the leaching of glycerol from the film in an aqueous environment and relatively large change in resistance when subjected to a large applied strain. Future materials development can include increasing the stability of plasticized agarose films in water by minimizing plasticizer leaching using a higher molecular weight compound. The electromechanical stability of the printed AgNW electrodes can also be improved by adding an encapsulation layer of biopolymer gel on the upper surface.

4. Experimental Section

Preparation of Agarose/Glycerol Gel Film Substrate: The agaroseglycerol gel film substrate that was used in this study was prepared by the solution casting method. 1% (w/v) agarose (BioReagent, molecular biology grade, low EEO, Sigma Aldrich, USA) solution was prepared by heating 0.2 g of agarose powder in 20 mL deionized water at 215 $^{\circ}$ C for 10 min on a magnetic stirrer (250 rpm). Then glycerol (99.5% assay, molecular weight 92.09 g mol⁻¹, Fisher Chemical, USA) was mixed at different ratios with different 1% (w/v) agarose solutions on the magnetic stirrer (250 rpm) in the ratios of 1:0.2, 1:0.5, 1:1, 1:3, 1:5, and 1:7 between agarose and glycerol. The solutions were then stirred until they became homogeneous, and cooled to \approx 50 °C. Then the cooled solutions were cast on square-shaped polystyrene petri dishes with sides of 100 mm (100 \times 15 mm). The solutions in the Petri dishes were left to dry on the workbench at room temperature (24 $^{\circ}$ C and \approx 50% relative humidity). The dried agarose-glycerol gel films were peeled off the Petri dishes after 4 days. The graphical representation of the process is shown in Figure 1b.

Printing AgNWs on Agarose/Glycerol Gel Film Substrate: The AgNWs used in this work were synthesized by a modified polyol method. [60] Typical screen printing was used to print customized AgNW ink. The mask with the desired printing pattern was fabricated by $\rm CO_2$ laser cutting PET sheet. The AgNW ink was formulated by mixing 4 wt.% AgNWs, into a polyethylene oxide (PEO) solution with 50% ethanol and 50% DI water as the solvent. After printing the AgNW patterns on the agarose/glycerol films, the printed electronics were dried on a hot plate at a temperature of 60 °C for 2 h to remove the solvent.

Characterizations: The UV-vis spectrum was measured by a UV-vis spectrophotometer, within the wavelength range of 200 to 800 nm. The FTIR spectrum of the agarose/glycerol gel films was measured by a Fourier transform infrared spectroscopy (FTIR; FT/IR-4200, JASCO) with a scan-

ning wavenumber range of 400 to 1000 cm⁻¹ using the typical KBr pellet method. 100 mg KBr powder was mixed with 2 mg ready-to-test pure agarose powder, pure glycerol, or agarose/glycerol gel films with different ratios. After grinding the mixer in mortar, the ground powder was pressed into a pellet and tested using a customized sample holder. The thermogravimetric (TGA) analysis was operated using TA Instruments Discovery SDT 650 with a heating rate of 5 °C min⁻¹ in a nitrogen atmosphere. In the static contact angle measurement, DI water, AgNW/ethanol suspension, and AgNW/terpineol/EC ink were used as the probe liquid, and a contact angle goniometer (Ramé-hart Instrument Co., Model 200-U1) was used to measure the contact angle at room temperature. The volume of the measured ink droplet was 5 μ L. To characterize the SEM image for the cross-section of printed AgNWs on agarose/glycerol substrate, the sample was nitrogen frozen and cut to expose the cross-section, and then the sample holder was tiled into 55° in the SEM (ThermoFisher Quanta 3D FEG) chamber.

Mechanical Evaluation: The tensile test was carried out using a tensile tester with a strain rate of $20~\mu m^{-1} s$. To measure the residual strain after the tensile stretching, the agarose/glycerol gel films with different ratios were cut into 3 cm \times 0.5 cm stripes and stretched by a customized tensile stage. Before stretching, the lengths of the stretched part were recorded. After one stretching-releasing cycle with a strain rate of $\approx \! 100~\mu m^{-1} s$, the samples were rested for 10 min to relax sufficiently. Then the length changes of the stretched parts were calculated, which can be considered as the residual of the samples after the tensile test.

Water Vapor Transmission Rate: The water vapor transmission rate of each agarose/glycerol gel film was measured on a homemade test system following the ASTM E96 standard. Specifically, a 20 mL-sized glass bottle was filled with 15 mL of distilled water, then sealed with a sample using Parafilm. The bottle with biopolymer gel films on it was placed in a chamber with a temperature of 35 °C and RH of 40% \pm 5%. The weight of the film was measured before sealing it on the bottle. The mass of the bottle with agarose/glycerol film on it was measured every 8 h. The water vapor transmission rate was calculated based on the mass change. And after 40 h of experiment, the tested agarose gel film was taken off and the weight was measured to calculate the weight change before and after the WVTR measurement.

Swelling by Weight and Volume: At first, the gel film was cut into a square shape (3 cm \times 3 cm) and weighed (W_i). The corresponding thickness (t_i) was measured. Then the film was submerged in 100 mL of deionized water and placed on the workbench at room temperature for 24 h. The swelling agarose gel film was taken out from the water at different time intervals, and the excess surface water was removed using Kimwipe paper. Each time the corresponding weight (W_f) was measured.

The swelling by weight (%) was calculated using Equation (1):

Swelling by weight (%) =
$$\frac{W_f - W_i}{W_i} \times 100\%$$
 (1)

where $W_{\rm i}$ and $W_{\rm f}$ are the weights of the square-sized gel film before and after swelling, respectively.

After 24 h of swelling, the length (a_f) , width (b_f) , and thickness (t_f) of the film were measured. The swelling by volume (%) was calculated using Equation (2):

Swelling by volume (%) =
$$\frac{a_i b_i t_i - a_f b_f t_f}{a_i b_i t_i} \times 100\%$$
 (2)

where $a_ib_it_i$ and $a_fb_ft_f$ are the volume of the agarose gel film before and after swelling.

Leaching Experiment: At first, the glycerol-plasticized agarose gel film was heated in an oven at 60 °C for 24 h to obtain the dry weight (W_1). The dry film was immersed in 100 mL of deionized water for 24 h which was placed at room temperature. Then the film was heated again in the oven at 60 °C for 24 h to obtain the dry weight (W_2) after the leaching of glycerol from the agarose gel film.

www.advelectronicmat.de

The dry weight loss of the film was calculated using Equation (3): program under award CMMI-2134664, and partial support from CMMI-

Dry weight loss (%) =
$$\frac{W_1 - W_2}{W_1} \times 100\%$$
 (3)

where W_1 and W_2 are the dry weights of the agarose gel films before and after the leaching of glycerol, respectively. A control experiment was performed using the same method to calculate the dry weight loss of an agarose film without any glycerol plasticizer.

Electromechanical Evaluation of the Printed Electronics: The resistance of the printed electronics was measured by a data acquisition system with a multimeter module (Keysight DAQ970A). The resistance change under cyclic loading-unloading tensile strain was measured using a customized step motor-controlled stage. The frequency of the cycles was set as 1 Hz. The electrode-skin impedance was measured by carrying out a frequency sweep using a potentiostat (Reference 600, Gamry Instruments) over a pair of electrodes placed at a distance of 2 cm on the forearm. The dry AgNW electrodes and commercial Ag/AgCl gel electrodes were placed at the same location for the test. To measure the electrode-skin impedance when the electrodes are under strain, the printed AgNW electrodes were pre-strained and mounted on the skin using a double-sided medical tape at the edge of the electrode (where there was no AgNW pattern).

ECG Measurement and EMG Human-Machine Interface Platform: The ECG system was set up using an AD8232 Module connected with an Arduino Nano BLE 33 evaluation board as the data acquisition platform. A typical three-electrode configuration was used, and the AgNW dry electrodes were connected to the board using ultrasoft enameled copper wires. The EMG sensor and human-machine interface were developed based on the AD8226 module. Arduino Nano BLE 33 was used to collect the rectified EMG signals and control an SG 90 servo motor. Three electrodes were mounted on the forearm, with two on the brachioradialis and the other on the back side of this muscle as the reference electrode. The "angry bird" was mounted on the rotating blade of the servo motor using double side tapes. When the motor moved under the control of the muscle, the figure falls.

Biodegradation of the Substrate and Recycling of the AgNWs: Before the biodegradation experiment, the electrodes of the sensor, the tweezer, and the Petri dish were first sterilized with 70% ethanol three times and dried. The microbial suspension was formulated by a commercially available compost accelerator (Roebic Bacterial Compost Accelerator) and probiotic additives (SCD Bio Ag), both of which contain a combination of natural microbes. More specifically, 0.5 g compost accelerator and 0.05 g probiotic additives were added to 50 mL DI water. Then the solution was allowed to rest at room temperature for 24 h and centrifuged to remove the solid particles of the compost accelerator. The supernatant was used to biodegrade the agarose/glycerol substrate. During the biodegradation experiment, the sample was immersed in the biodegradation solution and the temperature of the chamber was kept at 45 °C. The weight of the dried sample was measured termly along the experiment. The sterilization step was carried out after every weight measurement. On the 65th day, the floated microbial communities were removed by a dropper and the residual nondegraded substrate was taken out. The AgNW fragments were precipitated on the bottom of the Petri dish and collected. A centrifugation step with a slow rate of 200 rpm was carried out for the collected AgNWs in water to further remove the residue microbial communities. Then the AgNWs fragments were recycled to be redispersed in ethanol using our previously reported recycling strategy.[35]

Supporting Information

Supporting Information is available from the Wiley Online Library or from the author.

Acknowledgements

Y.L. and M.A. contributed equally to this work. The authors acknowledge the financial support of this research from the Future Manufacturing NSF

2233399.

Conflict of Interest

The authors declare no conflict of interest.

Data Availability Statement

The data that support the findings of this study are available from the corresponding author upon reasonable request.

Keywords

biodegradable substrates, electronic waste, recyclable metal nanowires, sustainable soft electronics

> Received: November 14, 2023 Revised: December 12, 2023 Published online: January 15, 2024

- [1] E. Hsu, K. Barmak, A. C. West, A.-H. A. Park, Green Chem. 2019, 21,
- [2] Z. Wang, B. Zhang, D. Guan, Nature 2016, 536, 23.
- [3] D. N. Perkins, M.-N. Brune Drisse, T. Nxele, P. D. Sly, Ann Glob Health 2014, 80, 286.
- [4] J. Li, H. Liu, J. Paul Chen, Water Res. 2018, 137, 362.
- [5] W. Wang, J. Wang, TrAC, Trends Anal. Chem. 2018, 108, 195.
- [6] L. Yin, H. Cheng, S. Mao, R. Haasch, Y. Liu, X. Xie, S.-W. Hwang, H. Jain, S.-K. Kang, Y. Su, R. Li, Y. Huang, J. A. Rogers, Adv. Func. Mater. 2014, 24, 645.
- W. Li, Q. Liu, Y. Zhang, C. Li, Z. He, W. C. H. Choy, P. J. Low, P. Sonar, A. K. K. Kyaw, Adv. Mater. 2020, 32, 2001591.
- [8] M. Irimia-Vladu, E. D. Glowacki, G. Voss, S. Bauer, N. S. Sariciftci, Mater. Today 2012, 15, 340.
- [9] M. Irimia-Vladu, Chem. Soc. Rev. 2014, 43, 588.
- [10] R. Li, L. Wang, D. Kong, L. Yin, Bioact Mater 2018, 3, 322.
- [11] Z. Zou, C. Zhu, Y. Li, X. Lei, W. Zhang, J. Xiao, Sci. Adv. 2018, 4, eaaa0508.
- [12] N. X. Williams, G. Bullard, N. Brooke, M. J. Therien, A. D. Franklin, Nat. Electron. 2021, 4, 261.
- [13] Y. H. Jung, T.-H. Chang, H. Zhang, C. Yao, Q. Zheng, V. W. Yang, H. Mi, M. Kim, S. J. Cho, D.-W. Park, H. Jiang, J. Lee, Y. Qiu, W. Zhou, Z. Cai, S. Gong, Z. Ma, Nat. Commun. 2015, 6, 7170.
- [14] S.-W. Hwang, J.-K. Song, X. Huang, H. Cheng, S.-K. Kang, B. H. Kim, J.-H. Kim, S. Yu, Y. Huang, J. A. Rogers, Adv. Mater. 2014, 26, 3905.
- [15] R. Bargagli, I. Mikhailova, in Monitoring with Lichens Monitoring Lichens, (Eds: P. L. Nimis, C. Scheidegger, P. A. Wolseley), Springer, Netherlands, 2002, pp. 65-84.</bib>
- [16] S.-R. Lim, J. M. Schoenung, J. Hazard. Mater. 2010, 177, 251.
- [17] R. Dagan, B. Dubey, G. Bitton, T. Townsend, Arch. Environ. Contam. Toxicol. 2007, 53, 168.
- [18] Y. Ding, S. Zhang, B. Liu, H. Zheng, C.-C. Chang, C. Ekberg, Resour Conserv Recycl 2019, 141, 284.
- [19] J. Cui, L. Zhang, J. Hazard. Mater. 2008, 158, 228.
- [20] Y. Liu, M. Zheng, B. O'connor, J. Dong, Y. Zhu, Sci. Adv. 2022, 8, eadd6996.
- [21] R. C. Webb, A. P. Bonifas, A. Behnaz, Y. Zhang, K. J. Yu, H. Cheng, M. Shi, Z. Bian, Z. Liu, Y.-S. Kim, W.-H. Yeo, J. S. Park, J. Song, Y. Li, Y. Huang, A. M. Gorbach, J. A. Rogers, Nat. Mater. 2013, 12, 938.

ADVANCED SCIENCE NEWS

www.advancedsciencenews.com



www.advelectronicmat.de

- [22] Y. Li, Y. Liu, S. R. A. Bhuiyan, Y. Zhu, S. Yao, Small Structures 2022, 3, 2100131.
- [23] J. Byun, Y. Lee, J. Yoon, B. Lee, E. Oh, S. Chung, T. Lee, K.-J. Cho, J. Kim, Y. Hong, Sci. Robot. 2018, 3, eaas 9020.
- [24] D. Son, J. Kang, O. Vardoulis, Y. Kim, N. Matsuhisa, J. Y. Oh, J. W. To, J. Mun, T. Katsumata, Y. Liu, A. F. Mcguire, M. Krason, F. Molina-Lopez, J. Ham, U. Kraft, Y. Lee, Y. Yun, J. B.-H. Tok, Z. Bao, *Nat. Nanotechnol.* 2018, 13, 1057.
- [25] C. Wang, H. Wang, B. Wang, H. Miyata, Y. Wang, M. O. G. Nayeem, J. J. Kim, S. Lee, T. Yokota, H. Onodera, T. Someya, *Sci. Adv.* 2022, 8, eabo 1396
- [26] H. Zhao, K. O'brien, S. Li, R. F. Shepherd, Sci Robot 2016, 1, eaai7529.
- [27] S. Wu, G. L. Baker, J. Yin, Y. Zhu, Soft Robot 2022, 9, 1031.
- [28] R. Kumar, J. Shin, L. Yin, J.-M. You, Y. S. Meng, J. Wang, Adv. Energy Mater. 2017, 7, 1602096.
- [29] S. G. Wallace, M. C. Brothers, Z. E. Brooks, S. V. Rangnekar, D. Lam, M. J. S. Lawrence, W. A. G. Rojas, K. W. Putz, S. S. Kim, M. C. Hersam, Eng. Res. Express 2022, 4, 015037.
- [30] Y. Liu, D. Shukla, H. Newman, Y. Zhu, Prog. Biomed. Eng. 2022, 4, 012001.
- [31] S. Yao, P. Swetha, Y. Zhu, Adv. Healthcare Mater. 2018, 7, 1700889.
- [32] H. L. Hernandez, S.-K. Kang, O. P. Lee, S.-W. Hwang, J. A. Kaitz, B. Inci, C. W. Park, S. Chung, N. R. Sottos, J. S. Moore, J. A. Rogers, S. R. White, Adv. Mater. 2014, 26, 7637.
- [33] T. Lei, M. Guan, J. Liu, H.-C. Lin, R. Pfattner, L. Shaw, A. F. Mcguire, T.-C. Huang, L. Shao, K.-T. Cheng, J. B.-H. Tok, Z. Bao, *Proc. Natl. Acad. Sci. USA* 2017, 114, 5107.
- [34] C. Shi, Z. Zou, Z. Lei, P. Zhu, W. Zhang, J. Xiao, Sci. Adv. 2020, 6, eabd0202.
- [35] Y. Liu, H. Wang, Y. Zhu, Adv. Electron. Mater. 2021, 7, 2100588.
- [36] A. K. Jaiswal, V. Kumar, E. Jansson, O.-H. Huttunen, A. Yamamoto, M. Vikman, A. Khakalo, J. Hiltunen, M. H. Behfar, Adv. Electron. Mater. 2023, 9, 2201094.
- [37] S. Chen, Z. Wu, C. Chu, Y. Ni, R. E. Neisiany, Z. You, Adv. Sci. 2022, 9, 2105146.
- [38] B. Deepa, E. Abraham, L. Pothan, N. Cordeiro, M. Faria, S. Thomas, J. Mater 2016, 9, 50.
- [39] P. Zarrintaj, S. Manouchehri, Z. Ahmadi, M. R. Saeb, A. M. Urbanska, D. L. Kaplan, M. Mozafari, M. Mozafari, Carbohydr. Polym. 2018, 187, 66

- [40] M. Bocqué, C. Voirin, V. Lapinte, S. Caillol, J.-J. Robin, J. Polym. Sci., Part A: Polym. Chem. 2016, 54, 11.
- [41] M. Khodadadi Yazdi, A. Taghizadeh, M. Taghizadeh, F. J. Stadler, M. Farokhi, F. Mottaghitalab, P. Zarrintaj, J. D. Ramsey, F. Seidi, M. R. Saeb, M. Mozafari, J. Controlled Release 2020, 326, 523.
- [42] P. Zarrintaj, B. Bakhshandeh, I. Rezaeian, B. Heshmatian, M. R. Ganjali, Sci. Rep. 2017, 7, 17187.
- [43] N. C. Stellwagen, J. Electrophor. 2009, 30, S188.
- [44] P. Blin, B. Boury, A. Taguet, J. Touja, L. Monconduit, S. Patra, Carbohydr. Polym. 2020, 247, 116697.
- [45] Q. Cao, Y. Zhang, W. Chen, X. Meng, B. Liu, Int. J. Biol. Macromol. 2018, 106, 1307.
- [46] V. Vivcharenko, A. Benko, K. Palka, M. Wojcik, A. Przekora, Int. J. Biol. Macromol. 2020, 164, 172.
- [47] Y. Hishikawa, E. Togawa, T. Kondo, ACS Omega 2017, 2, 1469.
- [48] Y. Luo, G. Zhou, L. Li, S. Xiong, Z. Yang, X. Chen, L. Huang, Fluid Phase Equilib. 2020, 518, 112626.
- [49] X. Zhao, Soft Matter 2014, 10, 672.
- [50] R. Ariati, F. Sales, A. Souza, R. A. Lima, J. Ribeiro, *Polymers* 2021, 13, 4258.
- [51] M. Kim, B.-U. Moon, C. H. Hidrovo, J. Micromech. Microeng. 2013, 23, 095024.
- [52] M. F. Griffin, B. C. Leung, Y. Premakumar, M. Szarko, P. E. Butler, Journal of Otolaryngology – Head & Neck Surgery 2017, 46. 33.
- [53] Z. Xue, H. Song, J. A. Rogers, Y. Zhang, Y. Huang, Adv. Mater. 2020, 32, 1902254.
- [54] S. Wu, Z. Cui, G. L. Baker, S. Mahendran, Z. Xie, Y. Zhu, ACS Appl. Mater. Interfaces 2021, 13, 59085.
- [55] W. Zhou, S. Yao, H. Wang, Q. Du, Y. Ma, Y. Zhu, ACS Nano 2020, 14, 5708
- [56] D. Shukla, Y. Liu, Y. Zhu, Nanoscale 2023, 15, 2767.
- [57] F. Xu, Y. Zhu, Adv. Mater. 2012, 24, 5117.
- [58] T. Wang, Y. Guo, P. Wan, H. Zhang, X. Chen, X. Sun, Small 2016, 12, 3748
- [59] M. Ahmad, M. Hasan, N. Tarannum, M. Hasan, S. Ahmed, Biosens Bioelectron X 2023, 14, 100375.
- [60] K. E. Korte, S. E. Skrabalak, Y. Xia, J. Mater. Chem. 2008, 18, 437.